Electron Leakage and Double-Exchange Ferromagnetism at the Interface between a Metal and an Antiferromagnetic Insulator: $CaRuO_3/CaMnO_3$

B. R. K Nanda,[1] S. Satpathy,[1,2] and M. S. Springborg[2]

[1]*Department of Physics, University of Missouri, Columbia, Missouri 65211, USA*

[2]*Universität des Saarlandes, Fachrichtung 8.1-Chemie, D-66041 Saarbrücken, Germany*

(Received 12 December 2006; published 22 May 2007)

Density-functional electronic structure studies of a prototype interface between a paramagnetic metal and an antiferromagnetic (AFM) insulator ($CaRuO_3/CaMnO_3$) reveal the exponential leakage of the metallic electrons into the insulator side. The leaked electrons in turn control the magnetism at the interface via the ferromagnetic (FM) Anderson-Hasegawa double exchange, which competes with the AFM superexchange of the bulk $CaMnO_3$. The competition produces a FM interfacial $CaMnO_3$ layer (possibly canted); but beyond this layer, the electron penetration is insufficient to alter the bulk magnetism.

DOI: 10.1103/PhysRevLett.98.216804 PACS numbers: 73.20.−r, 73.21.−b

Interfaces between perovskite oxides provide the exciting prospect for incorporating new correlated-electron physics, different from the standard semiconductor physics, into device applications. Recently a number of experimental groups have made considerable progress in fabricating high-quality oxide heterostructures and superlattices. In a recent work, Ohtomo *et al.* [1] reported the growth of atomically precise, lattice-matched superlattices made up of alternating layers of lanthanum and strontium titanates. This and other such experiments have raised the hope of opening up the oxide structures for new physics and potentially novel device concepts.

In this Letter, we study the electronic structure of a prototypical metal-on-antiferromagnetic-insulator interface, viz., $CaRuO_3/CaMnO_3$ (illustrated in Fig. 1) and show that the electrons from the metallic part leak out into the insulating part and modify the magnetism of the interface layer. The ferromagnetic double exchange of the leaked carriers competes with the antiferromagnetic superexchange producing a canted ferromagnetic state in the first $CaMnO_3$ layer. The electron leakage into the subsequent $CaMnO_3$ layers away from the interface is shown to be insufficient to alter the bulk antiferromagnetism. This structure has been recently grown and experimentally studied, [2] with a key finding that the ferromagnetism comes from the interface and is possibly canted, in agreement with our theoretical results.

The bulk electronic structures of both perovskite compounds are well known. $CaRuO_3$ is a paramagnetic metal [3] with the Ru ($t_{2g}^2\uparrow$, $t_{2g}^2\downarrow$) configuration and although it is believed to be close to a ferromagnetic instability [4,5]; this is not an important consideration here. $CaMnO_3$, on the other hand, is an AFM insulator, with the Mn ($t_{2g}^3\uparrow$) states occupied at each site [6,7]. The interface turns out to be very different from the two constituent bulks as indicated from our density-functional results. We studied the interface from density-functional theory (DFT) within the local spin-density approximation (LSDA), using the linear muffin-tin orbitals (LMTO-ASA) method [8]. The lattice mismatch between the two compounds is small (~2.9%), which helps the pseudomorphic growth, and, in this Letter, we have taken the idealized cubic lattice structure (a_{cubic} = 3.84 Å and 3.73 Å for the ruthenate and manganite, respectively) [9,10] ignoring the small orthorhombic distortions. The common lattice constant $a_\parallel$ along the plane of the interface was taken as the average bulk constant, while normal to the interface, $a_\perp$ was chosen so as to conserve the bulk volumes. Calculations were performed in the superlattice geometry for the five layer structure $(CaRuO_3)_5/(CaMnO_3)_5$. Test calculations of the structural relaxation near the interface using the LAPW method [11] showed very little change in the atom positions (<0.03 Å) and key physical quantities (see Fig. 3 for some results).

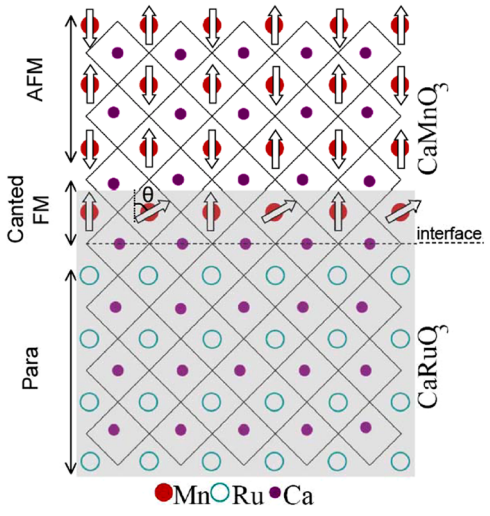

FIG. 1 (color online). Schematic structure of the $CaRuO_3/CaMnO_3$ interface, indicating a canted magnetic layer at the interface caused by the electron leakage (shown as the shadowed area) into the $CaMnO_3$ part.

We studied three different magnetic interfaces. For the AFM interface, all Mn atoms are in the type G structure as found in the bulk. For the FM interface, the first interfacial MnO_2 layer is ferromagnetic within the layer, with the remaining layers being type G AFM, while for the FM-II interface, the first two MnO_2 layers at the interface are ferromagnetic and the remaining layers are type G AFM. This choice of structures was based on the premise that electrons from the metallic ruthenate part would leak out into the manganite part and could turn the first few interfacial layers ferromagnetic via double exchange. We find that the FM interface has the lowest energy as indicated in Table I. As discussed later, this is consistent with the fact that the electrons from the metallic side do not penetrate beyond the first layer, so that the loss of superexchange energy caused by turning the second layer Mn atoms ferromagnetic is not compensated by a corresponding double-exchange gain of energy by the leaked itinerant electrons. Thus the magnetism of the first interfacial $CaMnO_3$ layer is modified, but the layers further away from the interface are not.

In Fig. 2, we show the layer projected densities of states (DOS) for the FM interface. The ruthenate layers are found to retain the paramagnetic character, except for the layer adjacent to the interface, which acquires a small ferromagnetic moment of about $0.03\mu_B$ per $CaRuO_3$ formula unit on account of its proximity to the interface. The most interesting feature is the first interfacial $CaMnO_3$ layer, which becomes metallic on account of leakage of electrons from the ruthenate part. Detailed analysis shows that the electron states at the Fermi energy in this layer consist mostly of Mn (e_g) states, with admixtures from the t_{2g} states. Analogous to the manganites physics, the e_g electrons will be treated as itinerant and the t_{2g} electrons as fixed core spins. The calculated Mn moment at the interface is slightly enhanced as compared to the bulk ($2.6\mu_B$ vs $2.4\mu_B$), which is consistent with the extra electrons being present at the interface $CaMnO_3$ layer.

To study the charge leakage into the manganite layers more quantitatively, we have computed the excess charge in each layer from the electron occupancy of the muffin-tin spheres. The atomic layers are organized as $\ldots(Ca^{2+}O^{2-})(Ru^{4+}O^{2-}{}_2)\ (Ca^{2+}O^{2-})\ (Ru^{4+}O^{2-}{}_2)\ [Ca^{2+}O^{2-}](Mn^{4+}O^{2-}{}_2)\ (Ca^{2+}O^{2-})\ (Mn^{4+}O^{2-}{}_2)\ (Ca^{2+}O^{2-})\ldots$, where each parenthesis denotes a layer parallel to the interface, while the square bracket denotes the nominal interface. Note that each individual atomic layer parallel to the interface being charge neutral, we have a nonpolar interface here and the issue of the divergence of the electrostatic potential for the polar interfaces [12], which is an important consideration for the $LaAlO_3/SrTiO_3$ interface [13,14], does not arise.

The excess charges for the individual layers, shown in Fig. 3, were computed by adding up the charges on atoms in that layer plus those of the two adjacent layers, to the left and the right, with 50% weight each, so that the procedure yields zero excess charge for the bulk. Note that beyond just a couple of layers on either side of the interface, the excess layer charge has reached zero, the bulk value, indicating that our chosen supercell is large enough to describe the isolated interface. The bottom panel of Fig. 3 shows the potential $V(z)$ felt by the electron, which was obtained from the potential at the muffin-tin sphere radius for the oxygen atoms in the CaO layers, common to both sides. The two important features clearly seen from the figure are the potential barrier at the interface as well as the exponential-like leakage of the electrons into the manganite part. For the sake of comparison, we have also shown in the bottom panel of Fig. 3 the Lang and Kohn [15] result for the electron density profile near a jellium surface corresponding to the electron-gas parameter $r_s = 3$, which is close to the value of 2.83, obtained by including the four Ru(d) electrons as forming the electron gas on the metallic side.

We have fitted the computed potential profile (Fig. 3) with a potential form relevant for the metal-insulator inter-

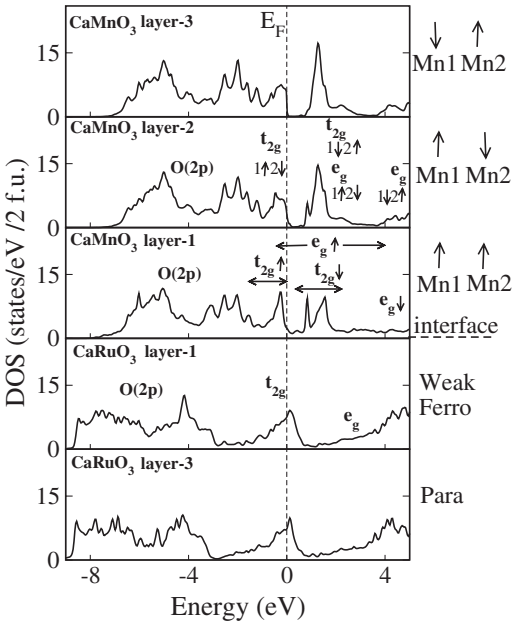

FIG. 2. Layer projected DOS for the FM interface of $(CaMnO_3)_5/(CaRuO_3)_5$. In this structure, the Mn moments at the interface layer are ferromagnetically aligned within the plane, while the remaining Mn moments are type G AFM (spin structures of the two inequivalent Mn atoms in each layer are indicated on the right). The leaked electrons from the ruthenate part produce a metallic and ferromagnetic $CaMnO_3$ layer (middle panel).

TABLE I. Calculated total energies, per interface Mn atom, for the $CaRuO_3/CaMnO_3$ interface, with three different magnetic structures as defined in the text.

Structure	AFM	FM	FM-II
Total energy	11 meV	0	63 meV

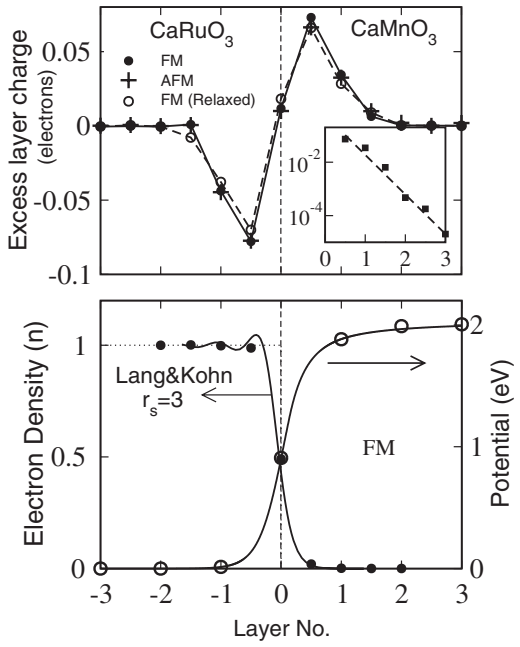

FIG. 3. Excess layer charge (top) and the electron density and potential profiles (bottom) at the interface. The electron density is normalized to the electron-gas density in the bulk ruthenate. The top panel also shows the excess charge with structural relaxation. In the bottom panel, the solid line with Friedel oscillations is the Lang and Kohn [15] result for the jellium model. The calculated potentials are shown as open circles, while the solid line is a fit using the Jones-Jennings-Jepsen surface model [16]. Inset in the top figure shows the exponential leakage of the electrons into the insulator side.

face, suggested by Jones, Jennings, and Jepsen [16] from the density-functional calculation of the tungsten surface. The potential, with the metal occupying the half-space $z < 0$,

$$V(z) = \begin{cases} 1 - \exp[-\lambda(z - z_0)]\}/[2\varepsilon_\infty(z - z_0)], & z > z_0 \\ U_0 - U_0/\{A \exp[-B(z_0 - z)] + 1\}, & z < z_0 \end{cases}, \tag{1}$$

has the image form away from the image plane z_0, where it is screened by the high-frequency dielectric constant ε_∞, and it has a smooth transition to the bulk potential, taken as zero, deep inside the metal. The constants A and B are not extra parameters, but are determined by matching the potential and its first derivative at the image plane z_0, where the potential has the value $-\lambda/(2\varepsilon_\infty)$. Using the measured value of the high-frequency dielectric constant for $CaMnO_3$ ($\varepsilon_\infty \approx 7$) [17], we find the fitting parameters to be $z_0 = 0.53$ Å (nominal interface $z = 0$ is at the CaO layer) and $\lambda = 1.6$ Å^{-1}. The value of B is 1.3 Å^{-1}, which describes how quickly the potential approaches the bulk value on the metallic side.

Although according to our DFT calculations, the energy of the FM interface layer is less than that of the AFM layer, the question still remains whether a canted magnetic state is even more favorable than the FM state. The itinerant e_g carriers leaked into the interfacial MnO_2 layer introduce a FM Anderson-Hasegawa double exchange [18], which competes with the existing AFM superexchange between the t_{2g} spins, leading to the possibility of a canted magnetic state, familiar from the physics of the colossal-magnetoresistive manganites physics.

To address this issue, we consider a lattice version of the Anderson-Hasegawa [18–21] Hamiltonian on a square lattice, as appropriate for the MnO_2 layer,

$$H = t \sum_{\langle ij \rangle \sigma} c^\dagger_{i\sigma} c_{j\sigma} + \text{H.c.} + \sum_{\langle ij \rangle} J\, \hat{S}_i \,.\, \hat{S}_j - 2J_H \sum_i \vec{S}_i \,.\, \vec{s}_i. \tag{2}$$

The model, restricted to the Mn sites, describes the motion of the itinerant electrons in a lattice of localized spins $\vec{S}_i$, with J being the superexchange and J_H being the Hund's coupling energy. The field operators for the itinerant e_g carriers are denoted by $c^\dagger_{i\sigma}$, $c_{i\sigma}$, where i and σ are the site and the spin indices, and $\vec{s}_i = (1/2)\sum_{\mu\nu} c^\dagger_{i\mu} \vec{\tau}_{\mu\nu} c_{i\nu}$ is the itinerant electron spin density, with $\vec{\tau}$ being the Pauli matrices. Guided by the earlier DFT calculations [6,22,23], the typical values of the Hamiltonian parameters for $CaMnO_3$ are: $t \approx -0.15$ eV, $J \approx 7$ meV, and $J_H \approx 1$ eV. We consider a square lattice consisting of two magnetic sublattices canted at an angle θ with respect to each other. Note that unlike our earlier work [21], here we neglect the on-site Coulomb energy between the itinerant carriers, since the number of carriers is small.

Working in a local spin quantization axis along the t_{2g} spin at each site, the one-particle wave functions are given by

$$\psi_{n\vec{k}} = \sum_{i\sigma} A_{n\sigma}(\vec{k})\, e^{i\vec{k}.\vec{r}}\, c^\dagger_{i\sigma}\, |0\rangle, \tag{3}$$

where n, $\vec{k}$ are the band index and the Bloch momentum and the band energies are given by the diagonalization of the 2×2 Hamiltonian matrix

$$H_k = \begin{bmatrix} \varepsilon_{\uparrow\uparrow}(k) & \Delta_{\uparrow\downarrow}(k) \\ \Delta_{\uparrow\downarrow}(k) & \varepsilon_{\downarrow\downarrow}(k) \end{bmatrix},$$

where $\varepsilon_{\uparrow\uparrow}(k) = 2t\, \cos(\theta/2)\, f(k)$, $\varepsilon_{\downarrow\downarrow}(k) = 3J_H - 2t\, \cos(\theta/2)\, f(k)$, and $\Delta_{\uparrow\downarrow}(k) = 2t\, \sin(\theta/2)\, f(k)$, with the function $f(k) = \cos k_x a + \cos k_y a$ being the tight-binding result for the square lattice. Denoting the number of nearest neighbors by ν, the total energy is given by

$$E = (\nu/2) J \cos\theta + \sum_{nk}^{occ} \varepsilon_{nk}. \tag{4}$$

The total energy as a function of the canting angle is shown in Fig. 4 for several values of the electron concentration x per lattice site. For the first layer with $x \approx 0.07$, the AFM state is indeed seen to be unstable to the formation of a canted state, while for the second interface layer, the AFM configuration within the plane has the

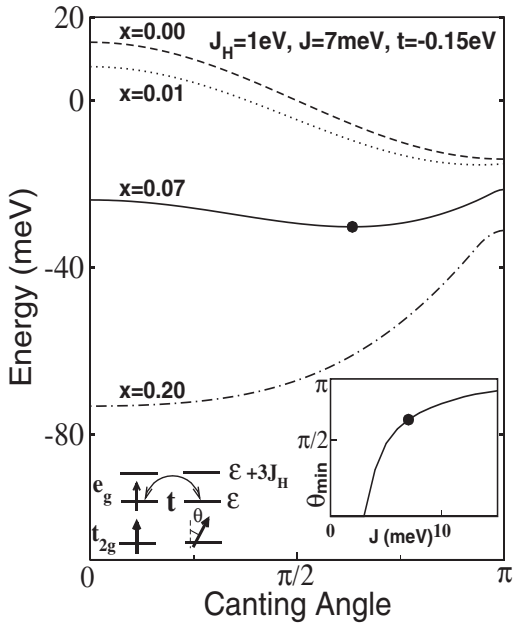

FIG. 4. Energy of a canted ferromagnetic state for a two-dimensional square lattice as a function of the canting angle θ. Inset shows the dependence of the canting angle $\theta_{\min}$ on the superexchange J for the itinerant carrier concentration of $x = 0.07$.

lowest energy, the electron leakage to that layer ($x \sim 0.01$) being insufficient to affect the magnetism. This is consistent with the *ab initio* density-functional energy shown in Table I, which showed that the second interface MnO_2 layer remains antiferromagnetic. The minimum for the canted state (shown by a dot in Fig. 4) is very shallow and thus while the model suggests that canting should occur, its exact magnitude would be sensitive to effects such as external pressure, interfacial stress, etc., which could change the Hamiltonian parameters by small amounts. The curve pertaining to $x = 0.2$ shows that the FM configuration is very quickly favored as the electron concentration is increased. Experiments [2] show an interfacial ferromagnetic moment of about $0.85\mu_B$ per interfacial Mn atom, from which by taking the moment to be $3\mu_B$ for the fully ferromagnetic case, we may estimate the experimental value for this canting angle to be about 115°, which is quite consistent with our model predictions shown in Fig. 4.

In summary, we have studied the interface $CaRuO_3$/$CaMnO_3$ between a prototypical paramagnetic metal and an antiferromagnetic insulator and have shown that the electrons leak into several layers of the antiferromagnetic part from the metallic part forming an exponential tail. The electron leakage to the first interfacial layer of the antiferromagnet is substantial enough to alter its magnetic properties, while there is virtually no effect on the magnetism of the layers further away from the interface. For the present case of $CaMnO_3$, the leaked electrons serve as itinerant carriers and alter the magnetism via the double-exchange mechanism, similar to the case of the electron doped manganite $La_xCa_{1-x}MnO_3$, where electrons are introduced due to La doping. The interface structure is of course different since the electrons are doped into just one interface layer instead of the entire bulk material. These results open up the intriguing prospect of tuning the interface magnetism through the control of the leaked carriers into the insulating layer.

This work was supported in part by the U. S. Department of Energy under Grant No. DE-FG02-00ER45818. One of us (S. S.) would like to acknowledge the German Science Foundation (DFG) for financial support.

[1] A. Ohtomo, D. A. Muller, J. L. Grazul, and H. Y. Hwang, Nature (London) **419**, 378 (2002).
[2] K. S. Takahashi, M. Kawasaki, and Y. Tokura, Appl. Phys. Lett. **79**, 1324 (2001).
[3] G. L. Catchen, T. M. Rearick, and D. G. Schlom, Phys. Rev. B **49**, 318 (1994).
[4] T. He and R. J. Cava, Phys. Rev. B **63**, 172403 (2001).
[5] I. I. Mazin and D. J. Singh, Phys. Rev. B **56**, 2556 (1997).
[6] S. Satpathy, Z. Popovic, and F. R. Vukajlovic, Phys. Rev. Lett. **76**, 960 (1996).
[7] S. Satpathy, Z. Popovic, and F. R. Vukajlovic, J. Appl. Phys. **79**, 4555 (1996).
[8] O. K. Andersen and O. Jepsen, Phys. Rev. Lett. **53**, 2571 (1984).
[9] H. Kobayashi, M. Nagata, R. Kanno, and Y. Kawamato, Mater. Res. Bull. **29**, 1271 (1994).
[10] J. B. A. A. Elemans, B. van Laar, K. R. van der Veen, and B. O. Loopstra, J. Solid State Chem. **3**, 238 (1971).
[11] P. Blaha *et al.*, *WIEN2k, "An Augmented Plane Wave + Local Orbitals Program for Calculating Crystal Properties"* (Karlheinz Schwarz, Techn. Universität Wien, Austria, 2001). ISBN .
[12] W. A. Harrison, E. A. Kraut, J. R. Waldrop, and R. W. Grant, Phys. Rev. B **18**, 4402 (1978); E. A. Kraut, Phys. Rev. B **31**, 6875 (1985).
[13] N. Nakagawa, H. Y. Hwang, and D. A. Muller, Nat. Mater. **5**, 204 (2006).
[14] S. Thiel *et al.*, Science **313**, 1942 (2006).
[15] N. D. Lang and W. Kohn, Phys. Rev. B **1**, 4555 (1970).
[16] R. O. Jones, P. J. Jennings, and O. Jepsen, Phys. Rev. B **29**, 6474 (1984); O. Jepsen and R. O. Jones, Phys. Rev. B **34**, 6695 (1986).
[17] N. N. Loshkareva *et al.*, Phys. Rev. B **70**, 224406 (2004).
[18] P. W. Anderson and H. Hasegawa, Phys. Rev. **100**, 675 (1955).
[19] C. Zener, Phys. Rev. **82**, 403 (1951).
[20] P.-G. De Gennes, Phys. Rev. **118**, 141 (1960).
[21] S. K. Mishra, S. Satpathy, F. Aryasetiawan, and O. Gunnarsson, Phys. Rev. B **55**, 2725 (1997).
[22] W. E. Pickett and D. J. Singh, Phys. Rev. B **53**, 1146 (1996).
[23] H. Meskine, H. Koenig, and S. Satpathy, Phys. Rev. B **64**, 094433 (2001).